Precipitation Behavior and Its Effect on Strengthening of an HSLA-Nb/Ti Steel

M. CHARLEUX, W.J. POOLE, M. MILITZER, and A. DESCHAMPS

The precipitation behavior of a commercial high-strength low-alloy (HSLA) steel microalloyed with 0.086 wt pct Nb and 0.047 wt pct Ti has been investigated using transmission electron microscopy (TEM) and mechanical testing. The emphasis of this study is to compare an industrially hot-rolled steel and samples from a laboratory hot torsion machine simulation. From TEM observations, the Ti and Nb containing precipitates could be grouped according to their size and shape. The precipitates in order of size were found to be cubic TiN particles with sizes in the range of 1 μm, grain boundary precipitates with diameters of approximately 10 nm, and very fine spherical or needle-shaped precipitates with sizes on the order of 1 nm. The needlelike precipitates were found on dislocations in ferrite and constituted the dominant population in terms of density. Thus, they appear to be responsible for the precipitation strengthening observed in this steel. Aging tests were carried out at 650 °C to evaluate the precipitate strengthening kinetics in detail. The strengthening mechanisms can be described with a nonlinear superposition of dislocation and precipitation hardening. The mechanical properties of torsion-simulated material and as-coiled industrial material are similar; however, there are some microstructural differences that can be attributed to the somewhat different processing routes in the laboratory as compared to hot strip rolling.

I. INTRODUCTION

THERE is currently a substantial interest in the development and use of high-strength steels for automotive applications with the goal to decrease vehicle weight. Over the last 30 years, high-strength low-alloy (HSLA) steels, *i.e.*, low-carbon steels microalloyed with Nb, Ti, and V, have become widely used in the automotive sector and also for pipeline applications. These steels derive their high strength from a combination of mechanisms including solid solution, grain size, dislocation, and precipitation hardening. State-of-the-art HSLA steels have a minimum yield strength of 550 MPa, and they are usually microalloyed with a combination of Ti and Nb. The Ti levels are sufficiently high that, after formation of TiN to remove N from solid solution, excess Ti is available to magnify the precipitation strengthening of fine carbides formed by the microalloying elements. The Nb additions play a critical role in delaying recrystallization during finish rolling.[1] Consequently, a pancaked austenite microstructure is formed, which results in promoting ferrite grain refinement during the subsequent austenite-to-ferrite transformation. Further, Mn alloying, typically of 1.5 wt pct, delays the austenite decomposition during accelerated cooling on the run-out table of a hot mill to sufficiently low transformation temperatures such that a quasi-polygonal ferrite microstructure forms.[2] This microstructure is characterized by the presence of very fine ferrite grains, *i.e.*, grain sizes of less than 3 μm and a significant number of transformation induced dislocations.[3,4]

To aid the consistent production of high-quality steels with low variation in mechanical properties, microstructure engineering has increasingly gained attention over the last two decades. Process models have been developed that link the operational parameters of a hot mill with the mechanical properties of the hot band based on the prediction of the microstructure evolution.[5,6,7] Initially, the modeling efforts emphasized controlled rolling due to delay of recrystallization by Nb. The Nb precipitation in austenite and its interaction with the recrystallization process have been investigated in detail.[1,8–11] More recently, modeling of the austenite decomposition on the run-out table and subsequent precipitation in ferrite have received increased attention reflecting the dominant significance of these phenomena in developing mechanical properties.[2,4,12–14] In particular, the precipitation strengthening model of Shercliff and Ashby[15] had been adopted for HSLA steels.[14]

However, current process models make still fairly simplified assumptions when dealing with the complex processes of carbide and nitride precipitation due to the additions of Nb and Ti as well as V or Al. Careful laboratory studies indicate that nucleation of NbC and TiC in austenite or ferrite requires heterogeneous nucleation sites such as grain boundaries, dislocations, or second-phase particles.[16] Interphase precipitation may form when the austenite-to-ferrite transformation takes place under slow cooling conditions.[17] For both interphase precipitation and precipitation in ferrite, the particles obey the Baker–Nutting relationship with the ferrite matrix. This criterion can therefore be used to distinguish between precipitation in austenite and the two other precipitation modes. Further, Kestenbach[18] related the various precipitation modes to the resulting precipitation strength by investigating NbC precipitation in a laboratory low-carbon steel containing 0.34 wt pct Nb. The results suggested a strengthening contribution of approximately 90

M. CHARLEUX, formerly Postdoctoral Fellow, The Centre for Metallurgical Process Engineering, University of British Columbia, is Research Engineer, ST Microelectronics, 38920 Crolles, France. W.J. POOLE, Associate Professor, and M. MILITZER, Assistant Professor, are with The Centre for Metallurgical Process Engineering, The University of British Columbia, Vancouver, BC, Canada V6T 1Z4. A. DESCHAMPS, Assistant Professor, is with Ecole Nationale Supérieure d'Electrochimie et d'Electrométallurgie de Grenoble, Institut National Polytechnique de Grenoble, 38402 St. Martin d'Hères, France.

Manuscript submitted August 18, 2000.

Table I. Chemical Composition of the Steel

Element	C	Mn	P	S	Si	Ti	Nb	Al	N
Wt pct	0.07	1.35	0.009	0.003	0.14	0.047	0.086	0.044	0.007
At. pct	0.33	1.37	0.016	0.005	0.28	0.055	0.052	0.091	0.028

MPa for precipitation on dislocations in ferrite and more than 200 MPa for interphase precipitation, and no strengthening effect was found for precipitation in austenite. In contrast, Itman *et al.*[19] assigned a strengthening contribution of 60 to 80 MPa to deformation-induced carbonitride precipitation in austenite for a commercially hot strip rolled steel, arguing that these precipitates remain fine because of the short processing time in the finishing mill. In summary, the origin and magnitude of precipitation strengthening in commercial microalloyed steels has still not been reliably established.

The rationale of the present work is to provide insight into the precipitation behavior of a state-of-the-art HSLA steel containing microalloying additions of Nb and Ti. The precipitation populations of an industrial processed coil and laboratory simulated material are examined in terms of their chemistry, morphology, size, and crystallography. Further, the strengthening mechanisms of these precipitates are analyzed by taking into account the interaction with dislocation hardening.

II. EXPERIMENTAL METHODOLOGY

The material investigated in this study is a Nb-Ti microalloyed commercial HSLA steel with a minimum yield strength requirement of 550 MPa. The chemical composition of this steel is given in Table I. The steel was obtained in the form of as-hot-rolled material coiled at 640 °C with a thickness of approximately 5 mm and transfer bar material with a thickness of approximately 30 mm.

The transfer bar material was used to machine specimens for simulation of hot strip rolling utilizing a DSI 100 HTS hot torsion machine where the temperature was monitored during the tests with a spot welded thermocouple. The simulation included a reheat period of 30 minutes at 1250 °C, three steps of deformation to simulate rough rolling at 1100 °C with an accumulated equivalent strain of 1.0, followed by five steps of deformation to simulate finish rolling starting at 1050 °C and finishing at 925 °C. For the finish rolling simulation, the strain per pass, deformation temperature, and interpass times were closely matched to the industrial process. However, a constant strain rate of 1 s^{-1} was used in the simulation, whereas strain rates of 5 to 200 s^{-1} were typical for the industrial process. Previous work has indicated that this difference in strain rate did not have a significant effect on the validity of the simulation.[20] Run-out table cooling was simulated by quenching the sample after the final deformation step using helium gas. The samples were quenched from 925 °C to room temperature. The average cooling rate for the torsion sample at a depth of 1 mm below the surface for the temperature range of 925 °C to 600 °C was 40 °C/s to 50 °C/s. This is similar to average cooling rates on the run-out table, which range from 10 °C/s to 100 °C/s depending on processing conditions such as spray bank activity, strip thickness, and strip speed. To simulate coiling, the samples subjected to torsion tests were reheated to 650 °C for 1 hour. Further, annealing treatments of 80 and 672 hours (4 weeks) were performed in order to examine the changes in precipitate size and shape. The as-hot-rolled coil material was also annealed for 80 and 672 hours at 650 °C. In all cases, the samples were sealed in a quartz tube under a roughing vacuum (10^{-3} Torr) and then annealed in an air furnace.

The simulated material was compared with the industrial material using optical microscopy, scanning electron microscopy (SEM), transmission electron microscopy (TEM), and by measurements of the mechanical properties. Samples for microscopy and mechanical property determination were taken from the middle part of the industrially processed coil. Microscopy samples from the torsion-simulated material were taken 1 mm from the surface of the sample. For optical metallography, the samples were etched in a 2 pct nital solution. The ferrite grain size was quantified by area measurements using an image analysis system. The grain size was characterized by an equivalent area diameter (EQAD).

The TEM studies were conducted on thin foils and carbon replicas. Thin foils were prepared as follows. First, 3-mm discs were ground to a thickness of ~60 to 70 μm using 1200 grit SiC grinding paper. These discs were then electropolished with a Struers Tenupol jet polisher using a solution of 95 pct glacial acetic acid and 5 pct perchloric acid at 70 V and a temperature of 15 °C. After electropolishing, the samples were rinsed in methanol before observations were conducted in a Hitachi H-800 (Hitachi Scientific Instruments, Mito City, Japan) transmission electron microscope operating at 200 kV. An important consideration for obtaining good images at high magnification is the magnetization of the TEM foil prior to loading into the electron microscope. This was accomplished by placing the foil in close proximity with a strong magnet as the final step before TEM examination. A drawback of this procedure is that very small amounts of tilt are available during subsequent observation; *i.e.*, if the sample is tilted more than a few degrees, the electron beam would demagnetize the sample and poor imaging conditions would return.

Carbon extraction replicas were prepared metallographically for chemical analysis by grinding the samples with various grinding papers down to 1200 grit and then polishing the surface with diamond paste (6 and 1 μm). The surface was then etched in 2 pct nital solution, and carbon was evaporated onto the surface under vacuum. Finally, the replica was removed with 5 pct nital solution and then cleaned in distilled water. The replicas were placed on copper grids before examination in the TEM. The precipitates in these replicas were chemically analyzed using a Hitachi H-800 in the scanning TEM–energy dispersive X-ray (EDX) mode and also with a JEOL* 2010 field emission gun TEM employing an EDX LINX analyzer. A drawback of carbon

*JEOL is a trademark of Japan Electron Optics Ltd., Tokyo.

Table II. Vickers Microhardness and Tensile Test Measurements for Coil and Simulated Material

Material	Hardness/VHN	Yield Strength/MPa	Ultimate Tensile Strength/MPa
Coil as received	241	648	720
Coil 80 h at 650 °C	208	553	626
Coil 672 h at 650 °C	184	455	519
Simulated as quenched	217	541	652
Simulated 1 h at 650 °C	254	675	752
Simulated 80 h at 650 °C	231	613	685
Simulated 672 h at 650 °C	207	553	619

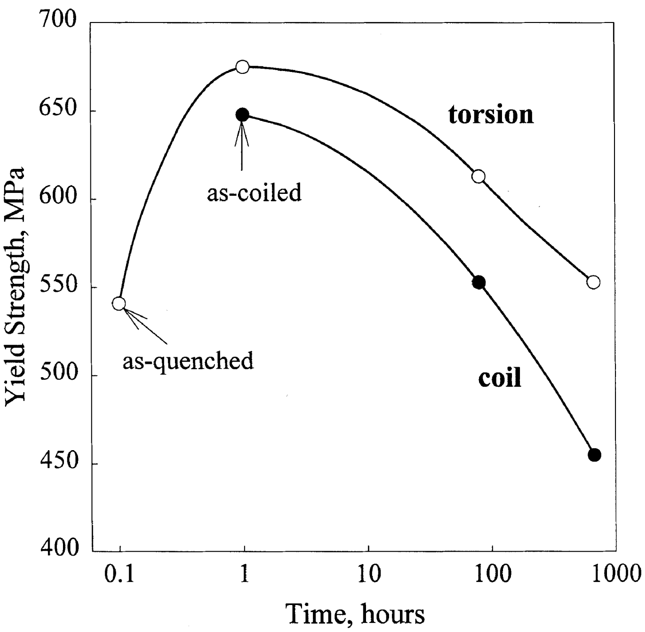

Fig. 1—Yield strength as a function of aging time at 650 °C; as-coiled material is shown as being aged for 1 h and the as-quenched material is shown at 0.1 h.

replicas is that no information on carbon content can be obtained.

Mechanical properties were obtained by Vickers microhardness measurements (500 g load) and by tensile testing of the samples using an MTS servohydraulic testing machine at a strain rate of 8×10^{-4} s^{-1}. For the tensile tests of the torsion samples, a special procedure had to be employed, as described by Hall and Worobec.[20] The center of the torsion sample where the microstructure is substantially different was drilled away to leave a homogeneous tubular sample, which was then tested in tension.

III. RESULTS

A. *Mechanical Properties*

The results from hardness and tensile tests are summarized in Table II. The yield strength is shown in Figure 1 as a function of aging time at 650 °C. For the simulated material, the yield strength first increases upon aging and reaches a peak strength after approximately 1 hour before decreasing upon further aging (Reference 2 provides more detailed discussion). These results are typical of classic precipitation hardening behavior. For the coil material, the situation is different because this material has already spent time at high temperatures during slow cooling of the coil; cooling to room temperature takes approximately 3 days. Previous results have shown that the peak strength is reached in the coiled material for a coiling temperature of approximately 650 °C.[2,4] Subsequently, the strength decreases during annealing, as shown in Figure 1.

Comparison between the simulated and coil material properties shows that the peak strength of the coil material is slightly lower than that of the simulated material, *i.e.*, 650 *vs* 675 MPa, respectively. Upon continued aging, the strength of both materials decreases at quite different rates such that, after 672 hours of overaging, the simulated and coil materials have a yield strength difference of almost 100 MPa; a similar trend can be observed for the ultimate tensile strength (Table II).

B. *Microstructure*

Optical micrographs of both materials are shown in Figure 2 for different aging times. All microstructures are predominantly ferritic. The as-received coil (Figure 2(a)) has a mixed microstructure consisting of many very fine grains with an EQAD in the range of 2 to 3 μm and a smaller number of much larger grains with an EQAD in the range of 20 to 30 μm. The grain boundaries appear irregular and the grains are elongated in the rolling direction. After aging for 672 hours at 650 °C, the same mixture of grains can be observed; however, the grain boundaries appear less irregular (Figure 2(b)). By conducting quantitative image analysis over an area of 100×100 μm counting approximately 1500 grains, an average grain size (EQAD) of 3 ± 0.5 μm is obtained for both conditions. While small differences were observed in the optical micrographs after annealing, these differences could not be quantifiably resolved.

The as-quenched microstructure of the simulated material is shown in Figure 2(c). The simulated material had a more nonpolygonal microstructure, but it also consisted of a mixture of very fine grains and a smaller number of larger grains. Further, as confirmed with higher magnification observations by SEM, very small pearlite colonies were seen (small darkly etched areas in Figure 2(c)), which were not observed in the coil material. Figure 2(d) demonstrates that, after annealing for 1 hour at 650 °C, the pearlite colonies were no longer visible, presumably due to spherodization. This is consistent with the observation that the pearlite colonies were not observed in the coil material as spherodization can readily occur during slow cooling after coiling. After 672 hours of annealing at 650 °C (Figure 2(e)), the grain boundaries appeared to be less irregular, a similar trend to that observed for the coil material. Again, average grain sizes (EQAD) of 3 ± 0.5 μm were found by quantitative image

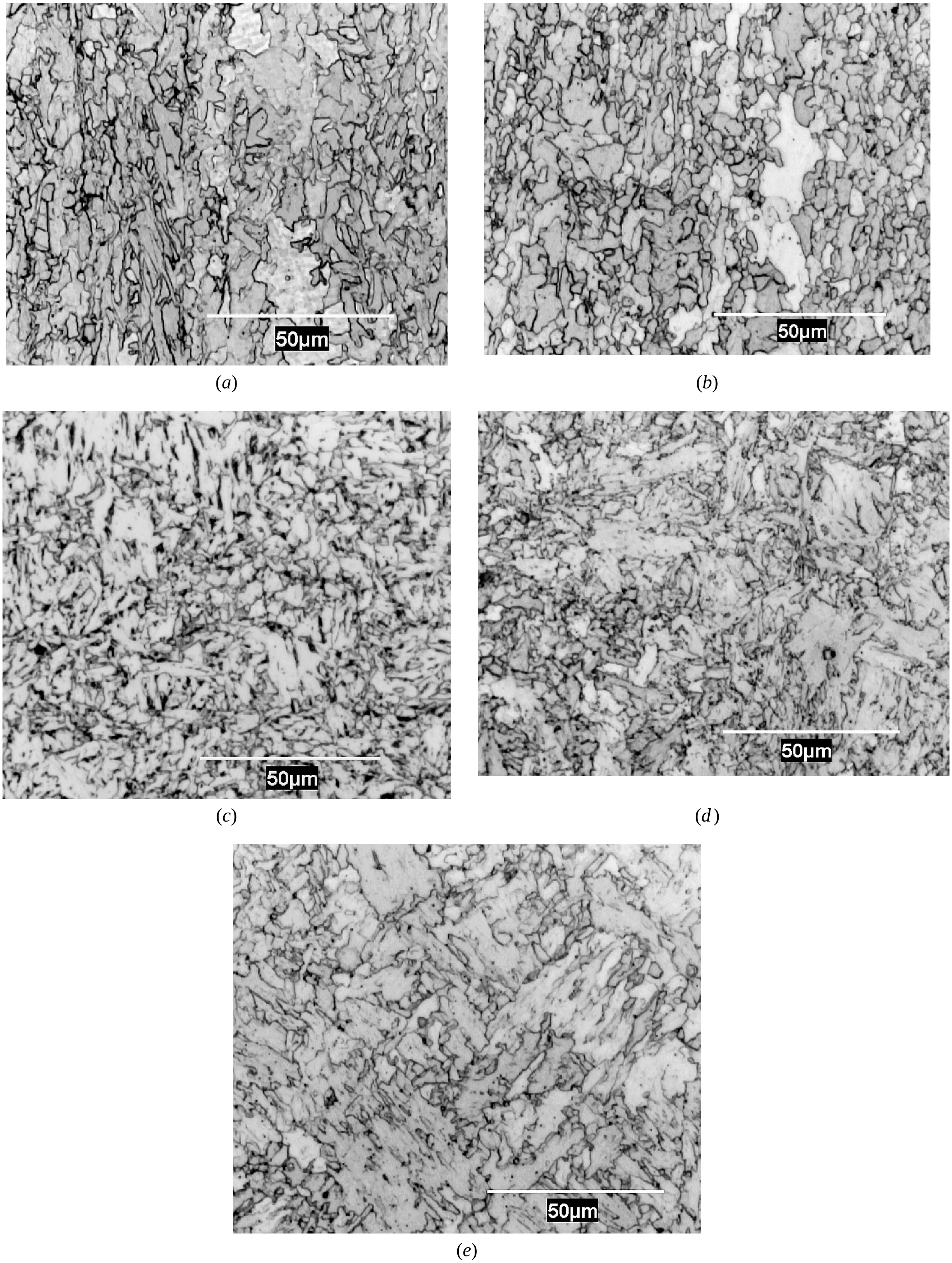

Fig. 2—Optical micrographs of (*a*) coil as received (rolling direction is in the vertical direction), (*b*) coil aged for 672 h at 650 °C, (*c*) simulated material as quenched, (*d*) simulated material aged for 1 h at 650 °C, and (*e*) simulated material aged for 672 h at 650 °C.

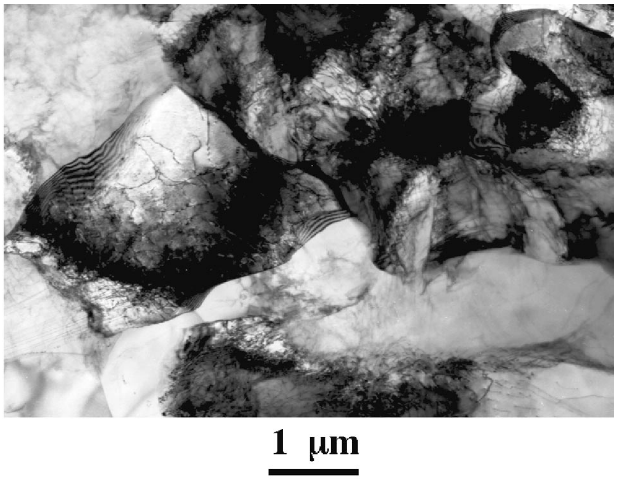

(*a*)

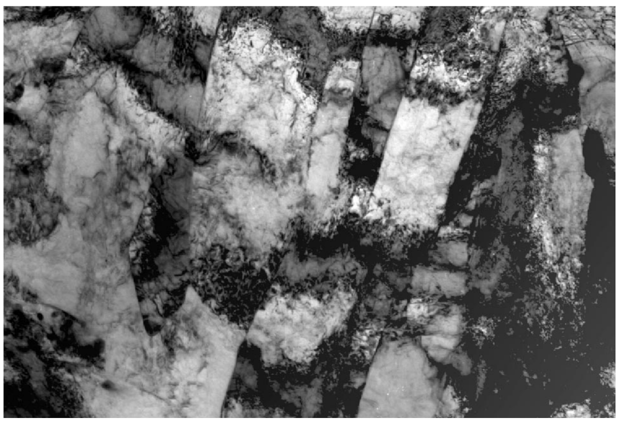

(*b*)

Fig. 3—TEM micrographs of (*a*) ferrite grains in the as-received coil and (*b*) the peak-aged torsion sample.

analysis; the qualitative changes in microstructure do not lead to a quantifiable change in the grain size within the error margin of the measurements.

The TEM observations show that the ferrite has a complicated structure for both the coil and simulated materials (Figure 3) with large variations from grain to grain. For the simulated material, a high density of dislocations was observed in all grains. The coil material was more complicated, as there was a mixture of grains with high dislocation densities as well as grains that appeared to be dislocation free. An order of magnitude measurement of the dislocation density was made in areas where a high density of dislocations was observed in the coil material. This was done by counting the number of dislocations in very thin regions of the foil near the edge of the hole. In this way, the dislocation density was estimated to be on the order of 10^{14} m^{-2}.

After annealing, a number of spherical Fe_3C precipitates, 0.1 to 0.5 μm in diameter, could be identified. Due to their relatively large size, these precipitates do not contribute to strengthening. The observation of large, spherical Fe_3C is consistent with the optical micrographs, which suggest that spherodization of the pearlite colonies occurred rapidly during annealing. Further, rows of relatively large precipitates could be seen, as shown in Figure 4. These precipitates were identified as containing niobium. It is presumed that these

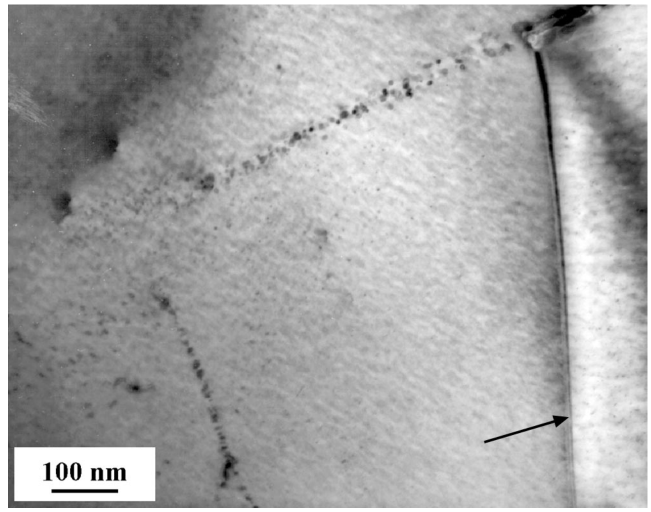

Fig. 4—TEM micrograph showing a line of precipitates at the prior ferrite grain boundary in the coil material aged for 80 h; arrow indicates current grain boundary location.

precipitates nucleated and grew on a ferrite grain boundary, which has subsequently migrated during annealing; the new location is marked by the arrow. The migration distance of the grain boundary is on the order of 0.3 to 0.5 μm. This is also consistent with the observations from optical microscopy that there was a local change in the shape of the grain boundary; *i.e.*, the grain boundaries became less irregular, although with very limited effect on the overall grain size, which had been measured with an accuracy of ± 0.5 μm, *i.e.*, within the margins of the migration distance.

C. *Precipitates*

The precipitates present in both the coil and simulated material were analyzed in terms of their chemistry, size, location, and morphology, as summarized in Table III. The largest precipitates observed are of square shape with a yellow/orange appearance in optical microscopy. These precipitates are referred to as type I. Figure 5(a) gives an example of one of the smaller ones of these precipitates, as observed by TEM. Their morphologies are typical of titanium nitride (TiN) precipitates.[21] The size of these precipitates was in the range of 200 to 2000 nm, and they were observed in both the coil and simulated material for all conditions. TiN precipitates are normally assumed to form in the melt prior to solidification. These particles are thermodynamically stable in austenite and ferrite and therefore will not dissolve during soaking or hot rolling. In the as-quenched simulated material, type I precipitates (TiN) are the only ones that are observed. In all other samples, a number of smaller precipitates can also be found.

The second type of precipitates, referred to as type II, is observed on grain and subgrain boundaries (Figure 5(b)). Their shape is more or less spherical. These precipitates, with a diameter of approximately 10 nm, contain niobium and titanium. They are unevenly distributed with some grain boundaries being free of precipitates.

Further, very fine precipitates are present, which, at the higher magnification, can be classified into two main types. The most numerous of these precipitates are needle shaped

Table III. **Typical Precipitates Containing Microalloying Elements Found in the As-Received Coil and the Simulated Material Aged for 1 Hour**

Type	Size Range/nm	Morphology	Location	Composition Identified (Type of Precipitate)
I	200 to 2000	square or polyhedral	random	Ti (TiN)
II	7 to 12	spherical	grain or subgrain boundaries	Nb + Ti (Nb/TiC)
III	length: 3 to 6 diameter: 0.7 to 0.9	needlelike	on dislocations in grains with high dislocation density	Nb + Ti (Nb/TiC)
IV	3 to 5 nm	spherical	in grains with low dislocation density	Nb + Ti (Nb/TiC)

(type III), while a smaller number of precipitates are spherical (type IV). Figure 5(c) shows a rare example where both types of precipitates are present in the same region. The emphasis of the investigation is focused on these smaller precipitates, which are assumed to be responsible for the observed precipitation hardening. The details of these small particles are described in the following.

A large density of small needle-shaped precipitates (type III) is observed in the coil and the simulated material. The needle shape of the precipitates can be seen directly in Figure 6, which shows examples of a typical dark-field image from the as-received coil as well as the torsion-simulated material aged for 1 hour at 650 °C. The streaking of the diffraction spots observed in the selected area diffraction patterns, which are shown as insets in Figure 6, is also consistent with the needle shape of the precipitates. The precipitates are mainly found along dislocation lines in the heavily dislocated ferrite grains. Figure 7 shows a higher magnification dark-field image from the overaged coil material, where the dislocation line and the needles are both in contrast. The crystallographic nature of the needles was determined from selected area diffraction patterns. The analysis of the diffraction pattern is complicated due to the large number of extraneous diffraction spots resulting from the surface oxide film. Nonetheless, the circled diffraction spot in Figure 6 is unambiguously attributed to the needles. The crystal structure of the precipitates was observed to be cubic and the lattice parameter was measured to be 0.41 nm. The crystallographic orientation of the precipitates with the ferrite matrix is $(100)_p//(100)_\alpha$ and $[011]_p//[010]_\alpha$, *i.e.*, the well-known Baker–Nutting relationship.[22] These basic crystallographic features of the precipitates remain constant throughout the aging process, although the diffraction spots lose their elongated nature as the precipitates increase their size. Usually, only one variant of these precipitates was observed in a given area, although in some cases, two variants could be observed.

The chemistry of the type III precipitates was examined using the replica technique on the overaged coil material. It was not possible to obtain chemical information on the smaller precipitates in the as-coiled or peak-aged materials. In the overaged samples, the metallic element composition is approximately 55 to 60 pct Nb/45 to 40 pct Ti for larger precipitates and 70 to 75 pct Nb/30 to 25 pct Ti for smaller ones. The EDX analysis indicated that nitrogen is not present in any of the precipitates examined.

During aging, the precipitates increase in size. Although quantification of precipitate sizes is difficult due to their very small length scale and the strain contrast around the precipitates, the following observations could be made. As illustrated in Figure 6, the precipitates sizes are similar in the as-received coil and the torsion sample aged for 1 hour; the needles are approximately 3 to 6 nm in length and 0.7 to 0.9 nm in diameter. With further aging, two effects can be observed, as shown in Figure 8. The overall precipitate size increases and the aspect ratio of the precipitates decreases. After 80 hours of aging, the precipitate size is 8 to 11 nm in length and 3 to 3.5 nm in diameter. Finally, after 672 hours of aging, the precipitates are 11 to 18 nm in length and 4 to 7 nm in diameter. Figure 9 shows some typical examples of precipitates in the overaged condition, where the precipitates are more ellipsoidal in shape rather than needlelike (*cf.* Figure 9(a)); some of the precipitates are almost spherical (*cf.* Figure 9(b)). Diffraction fringes can be observed perpendicular to the long axis of the precipitates showing that the orientation relationship between the matrix and the precipitates has been maintained.

Spherical precipitates (type IV) are occasionally found in the coil material, but these precipitates are not observed in the simulated material. The small spherical precipitates are located in ferrite grains with a low dislocation density, where they are arranged in curved lines, as shown in Figure 5(c). Based on a limited number of measurements, these precipitates contained niobium and titanium with niobium at a higher level, *i.e.*, 60 to 75 pct niobium. Due to the relative infrequency of such precipitates, further information regarding their crystallographic structure and their orientation relationship with the matrix has not been obtained.

IV. DISCUSSION

A. *Microstructure*

The microstructure of this steel is complicated with a heterogeneous distribution in dislocation density and the presence of precipitates of different sizes and morphologies. During aging, the possibility exists for precipitation, recovery of the dislocation substructure, and grain growth. There is little evidence of grain growth, although a noticeable trend is observed toward more regular grain boundaries during aging. Obviously, precipitation is the explanation for the initial strength increase in the simulated material. The drop in strength at longer aging times is more complicated and probably involves both recovery of the dislocation substructure and coarsening of precipitates.

Further, there are significant differences, both in terms of grain structure and yield strength, between the coil and the

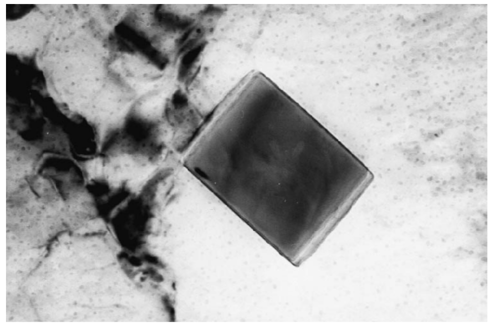

(*a*)

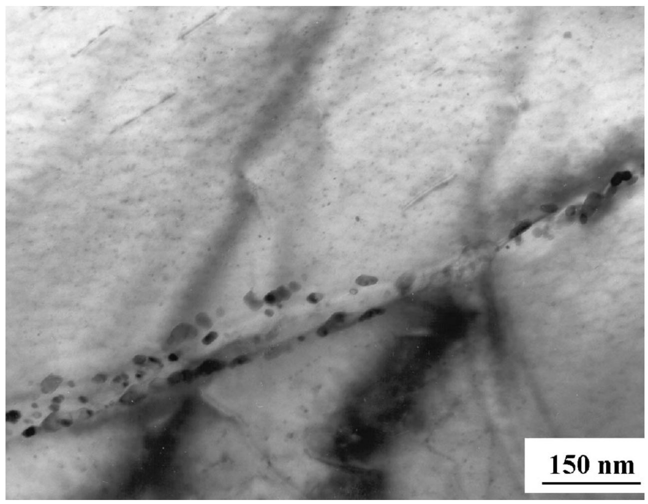

(*b*)

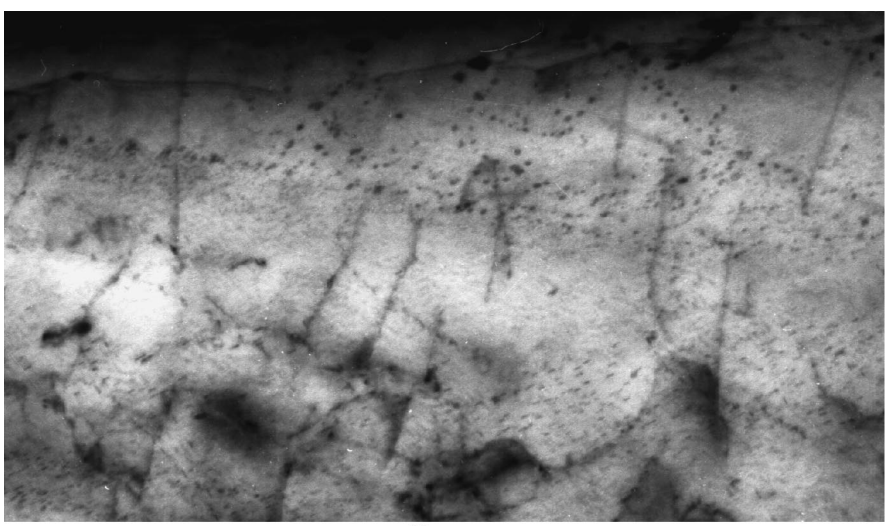

(*c*)

Fig. 5—Various types of precipitates encountered in the as-received coil: (*a*) TiN precipitates, (*b*) large (Nb,Ti)C precipitates at grain boundaries, and (*c*) fine round and needle-shaped (Nb,Ti)C precipitates.

simulated material. To understand these differences, it is important to examine the difference in processing for these materials. For the simulated material, the sample was cooled to room temperature in a continuous cooling path with a cooling rate of 40 °C/s to 50 °C/s in the temperature range of the austenite decomposition. In contrast, the coil material was rapidly cooled from austenite to the coiling temperature of 640 °C with a very slow subsequent cooling rate, initially on the order of 30 °C/h, during coiling. The resulting microstructures display the effect of the different cooling paths (*cf.* Figure 2). The simulated material has a predominantly nonpolygonal ferrite microstructure with islands of pearlite.

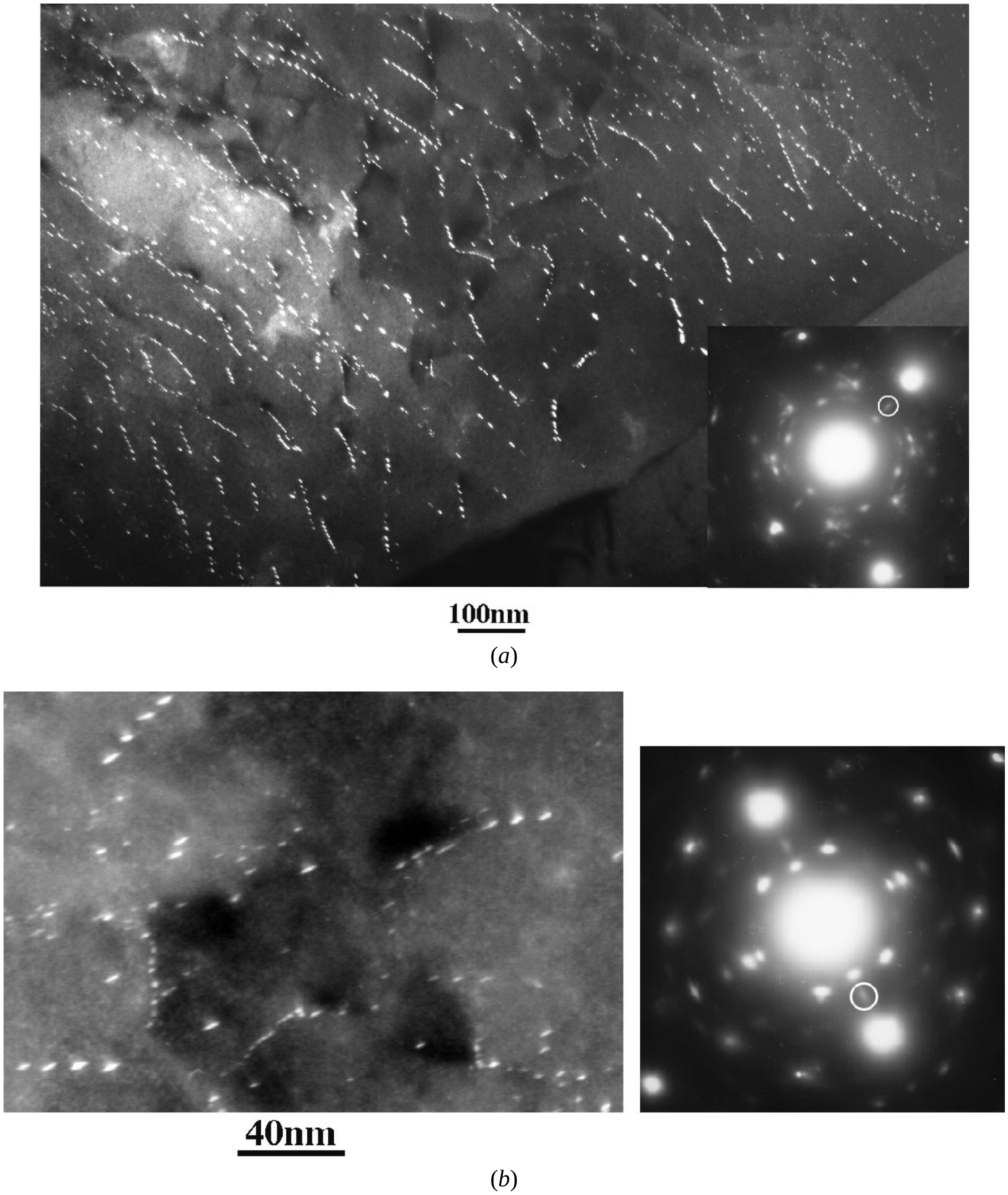

Fig. 6—Dark-field TEM micrographs and associated diffraction pattern for the needle-shaped precipitates: (*a*) as-received coil and (*b*) peak-aged torsion sample; the diffraction spots used for the dark fields are circled in white.

After 1 hour at 650 °C, the pearlite spherodizes and the differences between the microstructures of coil and simulated materials become less pronounced. However, the simulated material still appears to have a more nonpolygonal structure. This is also supported by the TEM observations where the coil material has a mixture of grains with high and low dislocation density, while the simulated material consists only of grains with a high dislocation density. These differences are related to the nature of the austenite decomposition. As transformation temperatures decrease, the formation of highly dislocated ferrite is promoted. In the torsion sample, the austenite-to-ferrite transformation is completed at significantly lower temperature than in the coil material, where the transformation is completed at 640 °C or above. Consequently, more highly dislocated ferrite is found in the torsion sample. The difference in microstructures affects not only the final grain structure but also the precipitation behavior, since nucleation of precipitates is strongly influenced by the presence of heterogeneous nucleation sites.

B. *Precipitates*

The observations made for precipitates are consistent with the fact that nucleation is confined to heterogeneous sites. In principle, precipitation of Nb/Ti carbides can occur in

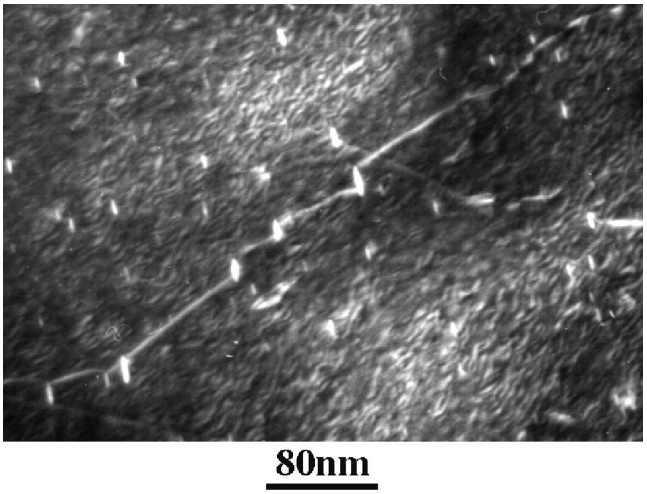

Fig. 7—Dark-field image of needle-shaped precipitates on a dislocation in the coiled material aged for 672 h.

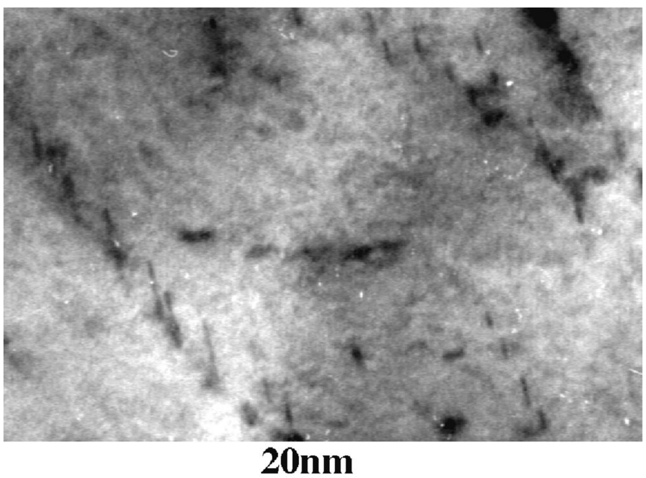

(*a*)

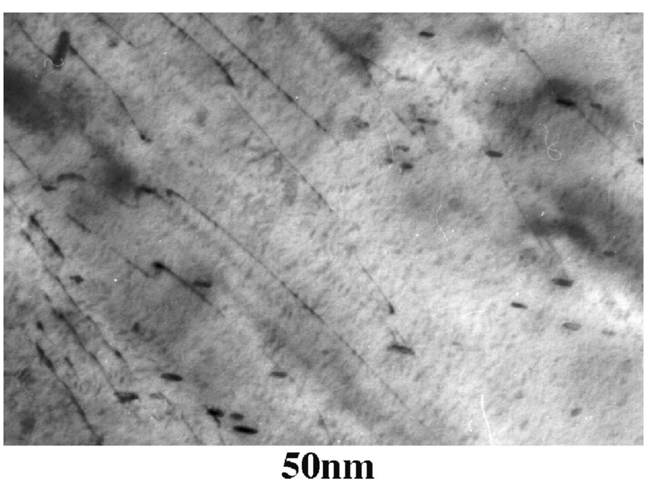

(*b*)

Fig. 8—Evolution of the needle-shaped precipitates with aging time for the coil material: (*a*) as received and (*b*) aged for 80 h.

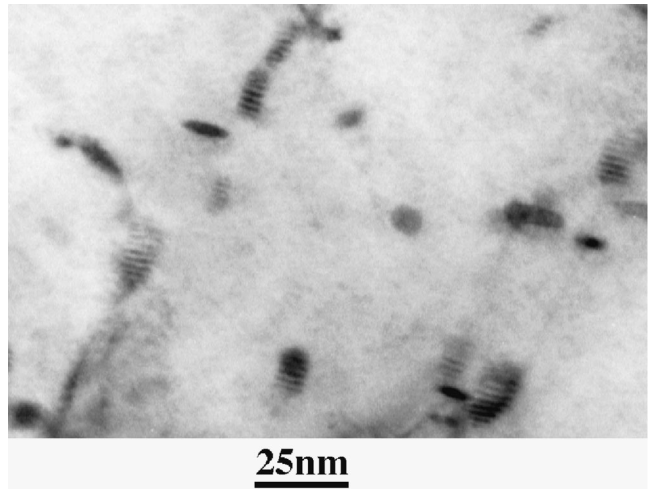

(*a*)

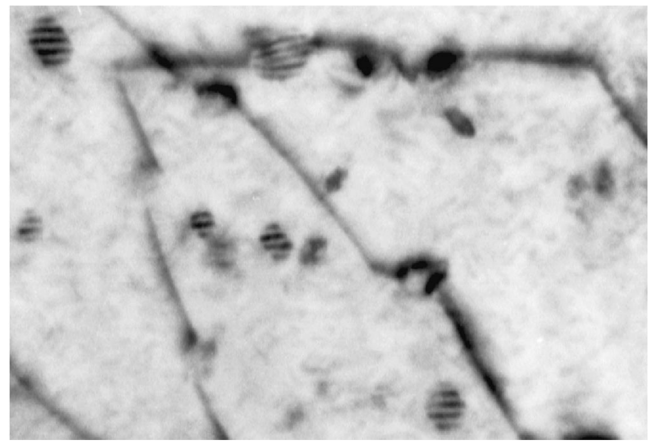

(*b*)

Fig. 9—Shapes of precipitates in the overaged state observed in the coil material aged for 672 h: (*a*) ellipsoidal shape and (*b*) spherical shape.

austenite or ferrite on grain boundaries, dislocations, subgrain boundaries or interphase boundaries during the austenite-to-ferrite transformation. Strain-induced precipitation of Nb carbides and/or carbonitrides in austenite has widely been discussed in the literature.[8–11] There is still controversy whether substantial Nb precipitation can occur during hot strip rolling with comparatively small processing times of the order of 10 seconds in the finishing mill. Some of the larger Nb/Ti carbides observed in the present work (*i.e.*, $>$10 nm) may have formed in austenite during the hot rolling process.

Interphase precipitation has generally been observed in slowly cooled steels.[17,18] For faster cooling rates, the velocity of the α/γ interface appears to be too high to allow for nucleation of precipitates at these interfaces. Essentially, nucleation is not possible when the interface has moved a distance greater than the critical nucleus size in the incubation time of nucleation.[23] Thus, the majority of the precipitates in the simulated material must have formed in ferrite. In the highly dislocated grains of this material, small needle-shaped precipitates along dislocation lines are the predominant observation. This finding is very similar to the results of Bošansky *et al.*,[24] who also found small needlelike precipitates in a similar alloy under welding conditions where high cooling rates promote the formation of heavily dislocated ferrite, *i.e.*, acicular ferrite or bainite.

For the coil material, the situation is more complex. In grains with high dislocation densities, the observations are similar to those made in the simulated material, *i.e.*, needle-shaped precipitates form along dislocation lines. For the relatively dislocation-free grains, either no precipitates or rows of small spherical precipitates are observed. For these precipitates, it is possible that (1) they result from an interphase precipitation occurring during the austenite-to-ferrite transformation when the velocity of the α/γ interface is quite low or (2) they nucleate on dislocations in austenite just prior to the austenite-to-ferrite transformation. This would explain their arrangement along curved lines when there is no evidence of corresponding dislocations in the ferrite. Unfortunately, it was not possible to identify the crystallographic orientation of the small spherical precipitates; *i.e.*, if they had obeyed the Baker–Nutting relationship, they would have had to be interphase precipitates.

The results from the coil material in the present study differ significantly from those of Pereloma and Boyd,[3] who studied a similar steel. In their work, the coil material also had a mixed microstructure of grains with high and low dislocation densities. However, they only observed fine spherical precipitates with diameters in the range of 15 to 30 nm. It is apparent from the present work that the precipitation process is very sensitive to the details of the austenite-to-ferrite transformation kinetics. Precipitation in ferrite is in general associated with the presence of highly dislocated grains. Otherwise, carbides only form as strain-induced precipitates in austenite or at the α/γ interface during slow cooling from the austenite phase field. Although the latter two processes are believed to be unlikely for hot strip, studies by Itman *et al.*[19] on the hot band of a steel containing 0.06 wt pct Ti and 0.02 wt pct Nb suggested otherwise. Based on their TEM observations, they suggested that carbonitrides in their steel nucleate only in austenite and, because of the short processing times, remain sufficiently small to still give a precipitation strengthening contribution of 60 to 80 MPa. This is not consistent with the present study, where precipitation strengthening is attributed to precipitates that must have formed in ferrite.

The observation that the type III precipitates in the overaged material do not contain nitrogen is consistent with the consideration that the nitrogen reacts with titanium in the melt to form TiN. For the investigated steel, there was a sufficient level of titanium alloy addition to tie up all the free nitrogen in the system by TiN formation. As a result, it can be expected that all the other observed precipitates will be nitrogen free. It therefore seems likely that these small precipitates are Nb/Ti carbides even though carbon presence has not been confirmed.

NbC and TiC both have crystal structures of the fcc NaCl type. In this work, the diffraction patterns from the precipitates were consistent with the NaCl crystal structure. However, the lattice parameter measured from the diffraction pattern is 0.41 ± 0.01 nm, somewhat lower than expected for bulk samples of TiC or NbC, *i.e.*, 0.433 nm for TiC and 0.447 nm for NbC.[25] In Nb/TiC, niobium and titanium are interchangeable in the lattice, resulting in a small change in lattice parameter. Based on measurements of composition (60 pct Nb-40 pct Ti)C, it would be estimated that the lattice parameter of the carbide should be equal to 0.44 nm, still larger than the value measured. However, it is possible that the presence of other elements such as Fe or Si in the precipitates could decrease the lattice parameter of the (Nb,Ti)C, thereby maintaining a good match with the matrix. Further, given the extremely small size of the needles, it is possible that significant elastic internal stresses are present in the precipitates in order to maintain coherency, although it seems unlikely that the total misfit strain could be accommodated in this manner. Finally, it should be noted that these results are not consistent with Bošansky *et al.*,[24] who reported a lattice parameter of 0.445 nm at the peak strength, or the results of Miglin *et al.*,[26] who measured a lattice parameter of 0.432 nm for spherical Ti/Nb carbonitrides. Further investigations are clearly necessary to clarify these discrepancies.

C. *Strengthening Mechanisms*

The relationship between mechanical properties and microstructure is complicated for this steel. The main strengthening mechanisms of relevance in this case are grain size strengthening, dislocation hardening, precipitation strengthening, and, to a lesser extent, solid solution hardening.

The base yield strength (in MPa) of the steel can be calculated in terms of the grain size and alloy additions from empirical relationships such as that developed by Choquet *et al.*[27] for plain low-carbon steels; *i.e.*,

$$\sigma_{\text{base}} = \sigma_0 + (15.4 - 30\text{C} + 6.094/(0.8 + \text{Mn}))d_\alpha^{-1/2}$$

with [1]

$$\sigma_0 = 63 + 23\text{Mn} + 53\text{Si} + 700\text{P}$$

where the concentrations are in weight percent and the ferrite grain size, d_a, is in millimeters. For the current steel chemistry, this gives a base strength of 405 MPa when a grain size of 3 μm is assumed. Further, assuming that the as-quenched sample of the simulated material represents the strength of the material in the absence of precipitation, it is possible to estimate the strengthening due to dislocation hardening resulting from the highly dislocated grains. The as-quenched yield strength is 540 MPa so that the dislocation contribution would be approximately 135 MPa. From this, the dislocation density may be estimated by

$$\sigma_{\text{dis}} = \alpha M G b \sqrt{\rho} \qquad [2]$$

where α is a constant, M is the average Taylor factor, b is the magnitude of the Burgers vector, G is the shear modulus, and ρ is the dislocation density. Using typical values for iron (*i.e.*, $\alpha = 0.3$, $M \approx 3$, $G = 64$ GPa, and $b = 0.25$ nm),[28,29] an average dislocation density of 9×10^{13} m^{-2} would be associated with the required yield strength contribution. This result is similar to the estimate of 10^{14} m^{-2} for the dislocation density made from TEM observations.

Evaluating the contribution due to precipitation hardening is considerably more complicated. However, in the simulated material, precipitation primarily consists of Nb/Ti carbides nucleated on ferrite dislocations. To estimate hardening associated with these precipitates, the following is required: (1) volume fraction of precipitates, (2) size and shape of precipitates in order to calculate the mean precipitate spacing, (3) strength of precipitates as obstacles to dislocations and how dislocations sample the obstacles, and (4) flow stress addition laws for combining dislocation and precipitation hardening. Several researchers have proposed that the Orowan–Ashby equation is appropriate for analyzing precipitation hardening in these systems.[17–19,30] For many cases, this approach is well justified and gives good estimates. In the present case, the small size of the precipitates at the peak strength indicates that precipitates would almost certainly be shearable, and therefore, the Orowan–Ashby equation, which assumes nonshearable precipitates, cannot be used. An estimate of the shearable/nonshearable transition diameter, D_t, can be made by considering the smallest precipitate that can support a dislocation loop. The maximum strength of the precipitate is given by its theoretical strength, *i.e.*, $G_{ppt}/30$,[31] where G_{ppt} is the shear modulus of the precipitate. The stress to support a dislocation loop is given by

$$\tau = \frac{Gb}{D_t} \quad [3]$$

where a line tension of $0.5Gb^2$ is assumed. Equating the stress from the dislocation loop to the theoretical strength gives

$$D_t = \frac{30Gb}{G_{ppt}} \quad [4]$$

Assuming a rule of mixture, the shear modulus of 60 pct Nb-40 pct Ti particles is approximately 150 GPa (180 GPa for TiC and 135 GPa for NbC),[32] yielding a diameter of 4 nm. This estimate is in agreement with Gladman, who recently suggested that the shearable/nonshearable transition diameter is approximately 5 nm.[30]

The likelihood that the precipitates in the present case are substantially smaller than the shearable/nonshearable transition diameter considerably complicates the analysis of strengthening due to precipitation. However, the following simplified approach may be taken. For relatively weak precipitates such as these, the appropriate precipitate spacing of the dislocation samples is given by the Friedel spacing, and therefore, the strengthening in a polycrystal is given by[33]

$$\sigma_{ppt} = \frac{2M}{bLT^{1/2}}\left(\frac{F}{2}\right)^{3/2} \quad [5]$$

where L is the average interprecipitate spacing, T is the line tension of the dislocation, and F is the strength of the precipitate as an obstacle. The strength of the obstacle relative to a nonshearable precipitate can be defined by

$$\Gamma = \frac{F}{2T} \quad [6]$$

where the strength of a nonshearable obstacle is $2T$ with $T = 0.5Gb^2$. The spacing of precipitates on the slip plane, *i.e.*, the intersection of the needles with the slip plane, may be calculated by modifying the approach described by Gladman[34] to give

$$L = \frac{\pi^{1/2} D}{2f^{1/2}} \quad [7]$$

where D is the diameter of the needles and f is the volume fraction of precipitates. Consequently,

$$\sigma_{ppt} = \frac{2MGbf^{1/2}}{\pi^{1/2}D}\Gamma^{3/2} \quad [8]$$

is obtained. It is difficult to estimate the relative obstacle strength, Γ, of the precipitate *per se*. Thus, it is proposed to determine Γ from the precipitate contribution at the experimentally measured peak strength taking into account the estimates of (1) base strength and (2) dislocation hardening. However, to extract a precipitation strength contribution, the appropriate addition laws for summing the strengthening components have to be considered. This problem has received considerable attention from a fundamental point of view.[33,35] It is necessary to consider the relative length scales and relative strength of the strengthening obstacles. If these are significantly different, a linear addition is appropriate. For example, the base strength of the alloy derives from solid solution hardening and grain size strengthening. The appropriate length scales for these processes are very different so that a linear addition law should be used, as in Eq. [1]. On the other hand, precipitation and dislocation hardening arise from a similar density and strength of obstacles, which dislocations sample on the glide plane. Using computer simulations, Foreman and Makin[35] obtained a Pythagorean flow stress addition law for discrete obstacles on the slip plane in the case where a similar density of relatively strong discrete obstacles (*e.g.*, forest dislocations) and relatively weak obstacles (*e.g.*, precipitates) is present. Applying their analysis to the present case, it is therefore appropriate to use the following relationship for the yield strength:

$$\sigma_{ys} = \sigma_{\text{base}} + (\sigma_{dis}^2 + \sigma_{ppt}^2)^{1/2} \quad [9]$$

Employing the experimentally determined value for the yield strength at the peak strength and substituting the estimates for the base strength and dislocation strengthening, the precipitation hardening contribution is 234 MPa.

The volume fraction of strengthening precipitates is the sum of the volume fractions of NbC and TiC precipitates, which may be calculated using the relationships of Gladman.[34] Due to the low solubility of Nb and Ti in ferrite,[36] it is assumed that all Nb and Ti is precipitated at the peak strength. A volume fraction of 0.0014 is obtained taking into account that only the excess Ti after TiN precipitation is available for TiC formation. Then, adopting the measured precipitate diameter, *i.e.*, 0.8 nm,* the strength of the precipitates as obstacles can be obtained from Eq. [8]; *i.e.*, $\Gamma = 0.18$. In other words, the precipitates possess approximately 20 pct of the nonshearable strength. This is a reasonable result for the precipitate strength considering a nonshearable diameter of 4 to 5 nm.

Clearly, a number of assumptions had to be made in order to evaluate the precipitation strengthening. Nonetheless, the basic strengthening mechanisms observed in the steel can be understood semiquantitatively. The ability to make predictions is limited due to the uncertainties in the estimates of the shearable-nonshearable transition radius. It would be useful to have more detailed experimental studies over a wider range of conditions to verify the consistency of the present observations. Presently, only extremely labor-intensive *in-situ* transmission electron microscopy on lightly deformed samples, *i.e.*, where the dislocations have been

*Relevant diameter for needles is the cylinder diameter.

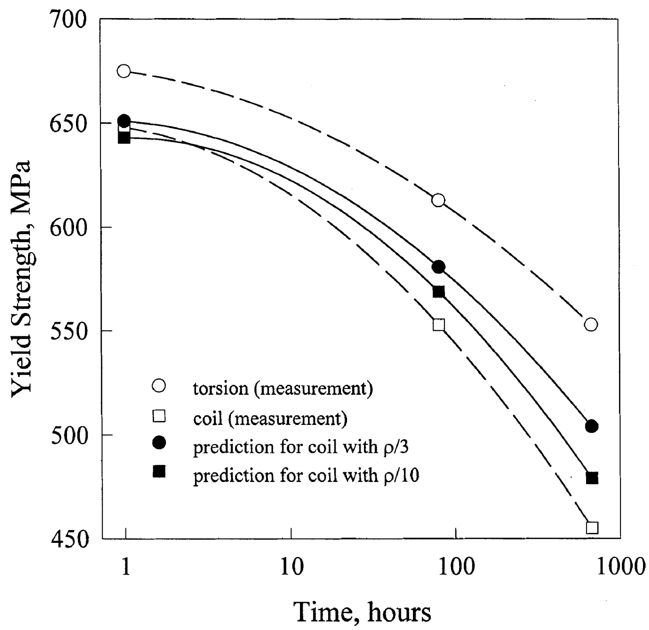

Fig. 10—Overaging behavior of coil and torsion material; predictions assume a lower dislocation density in the coil with 1/3 and 1/10 of the dislocation density, ρ, of the torsion material, respectively.

pushed between the obstacles, may give some qualitative information on the appropriate relationship between breaking angle and precipitate diameter.[37]

During overaging, the situation is even more complicated, as recovery of the dislocation substructure has to be considered. Furthermore, the recovery process may be strongly linked to the precipitation kinetics, since the precipitates may act as pinning sites on the dislocation lines limiting the ability of dislocations to rearrange themselves into lower energy configurations.

The difference in mechanical properties between the industrially processed material and the laboratory simulated material can be rationalized in terms of the observed differences in microstructures. The coil material has a similar grain size but a lower overall dislocation density due to the mixture of low and high dislocation density grains. Based on the order of magnitude approximations for the dislocation density, the peak precipitation strengthening contribution in the coiled material can be estimated from the as-received yield strength. For this estimation, a base strength of 405 MPa can be adopted as for the torsion material. Dislocation densities are considered, which are half an order of magnitude and one order of magnitude, respectively, smaller than in the torsion sample. Then a maximum precipitation strength of 230 and 239 MPa is obtained, which is similar to that of the peak-aged torsion sample. Further, coarsening of the precipitates in coil and torsion materials proceeds in a very similar manner, as shown by the TEM investigations. Neglecting recovery for simplicity, precipitation strength decreases to 158 and 61 MPa during overaging for 80 and 672 hours, respectively, as calculated from the yield strength data of the simulated material employing Eq. [9]. Adopting these values together with the lower dislocation densities, a more rapid overaging is then predicted for the coil samples, as illustrated in Figure 10. Thus, the divergence between the strength levels during overaging is attributable to the difference of dislocation hardening. For quantitatively more accurate descriptions, changes in dislocation densities due to recovery would have to be considered.

V. CONCLUSIONS

Microstructures and properties have been analyzed for a state-of-the-art 550 MPa HSLA steel. The significance of precipitation strengthening and its interaction with dislocation hardening has been determined by comparing industrially processed and laboratory simulated materials. The strengthening precipitates have been identified as very fine needles of Nb/Ti carbides in both materials. Nucleation and growth of these needles predominately occur on ferrite dislocations. The precipitates are too small to be nonshearable such that the Orowan–Ashby model cannot be used to determine precipitation strength. A nonlinear flow stress addition law has been adopted to describe the combined strengthening contribution of precipitates and dislocations. In addition to the precipitation behavior, the ferrite grain sizes are similar in both materials. Consequently, mechanical properties obtained from the torsion simulation of industrial hot rolling are similar to those measured in the industrial material. For example, the yield strength of the torsion-simulated material is 25 MPa (approximately 4 pct) larger than that of the industrially hot-rolled material. These results confirm torsion tests as an excellent simulation tool for industrial hot rolling operations.

In spite of these favorable simulation results, further examinations reveal some substantial differences in the microstructure and associated overaging behavior of simulated and industrial materials. In the torsion sample, all ferrite grains are highly dislocated, whereas in the industrial material, a mixture of highly dislocated ferrite and low dislocation density ferrite is observed. This observation is consistent with the 4 pct larger yield strength of the torsion sample. To avoid these slight differences, torsion simulations should replicate the industrial cooling pattern more accurately by implementing a stepped cooling regime rather than cooling the specimens to room temperature before simulating coiling with an isothermal heat treatment. This would facilitate a better match of the transformation temperatures for the austenite decomposition in the laboratory to those on the run-out table.

Further, an improved predictive capability of the structure-property relations requires more detail regarding the evolution of dislocation densities during aging and the consideration of the complexity of mixed microstructures. Improvements along these lines appear also to be critical for the investigation of novel high-strength multiphase steels, where transformation hardening constitutes an essential strength contribution.

ACKNOWLEDGMENTS

The authors acknowledge the financial support received from the American Iron and Steel Institute (AISI) and the United States Department of Energy (DOE). The assistance of Xiande Chen, who conducted the torsion tests, is gratefully appreciated.

REFERENCES

1. I. Tamura, H. Sekine, T. Tanaka, and C. Ouchi: *Thermomechanical Processing of High Strength Low Alloy Steels*, Butterworth and Co., London, 1988.
2. M. Militzer, E.B. Hawbolt, and T.R. Meadowcroft: *Metall. Mater. Trans. A*, 2000, vol. 31A, pp. 1247-59.
3. E.V. Pereloma and J.D. Boyd: *Mater. Sci. Technol.*, 1996, vol. 12, pp. 808-17.
4. M. Militzer, D.Q. Jin, and I.V. Samarasekera: in *Advances in Industrial Materials*, D.S. Wilkinson, W.J. Poole, and A. Alpas, eds., The Metallurgical Society of CIM, Montreal, 1998, pp. 63-77.
5. C.M. Sellars and J.A. Whiteman: *Met. Sci.*, 1979, vol. 13, pp. 187-94.
6. P.D. Hodgson and R.K. Gibbs: *Iron Steel Inst. Jpn. Int.*, 1992, vol. 32, pp. 1329-38.
7. I.V. Samarasekera, D.Q. Jin, and J.K. Brimacombe: *38th Mechanical Working and Steel Processing Conf. Proc.*, ISS, Warrendale, PA, 1997, vol. XXXIV, pp. 313-27.
8. B. Dutta and C.M. Sellars: *Mater. Sci. Technol.*, 1987, vol. 3, pp. 197-206.
9. W.P. Sun, M. Militzer, D.Q. Bai, and J.J. Jonas: *Acta Metall. Mater.*, 1993, vol. 41, pp. 3595-3604.
10. S.F. Medina: *Mater. Sci. Technol.*, 1998, vol. 14, pp. 217-21.
11. S.F. Medina and J.E. Mancilla: *Acta Metall. Mater.*, 1994, vol. 42, pp. 3945-51.
12. J. Andorfer, D. Auzinger, B. Buchmayr, W. Giselbrecht, G. Hribernig, G. Hubmer, A. Luger, and A. Samoilov: in *Thermec '97*, T. Chandra and T. Sakai, eds., TMS, Warrendale, PA, 1997, pp. 2069-75.
13. A. Prasad, S. Jha, and N.S. Mishra: *Steel Res.*, 1995, vol. 66, pp. 416-23.
14. M. Militzer, W.J. Poole, and W.P. Sun: *Steel Res.*, 1998, vol. 69, pp. 279-85.
15. H.R. Shercliff and M.F. Ashby: *Acta Metall. Mater.*, 1990, vol. 38, pp. 1789-1802.
16. A.J. DeArdo, J.M. Gray, and L. Meyer: in *Niobium*, H. Stuart, ed., TMS-AIME, Warrendale, PA, 1984, pp. 685-759.
17. R.M. Brito and H.J. Kestenbach: *J. Mater. Sci.*, 1981, vol. 16, pp. 1257-63.
18. H.J. Kestenbach: *Mater. Sci. Technol.*, 1997, vol. 13, pp. 731-39.
19. A. Itman, K.R. Cardoso, and H.J. Kestenbach: *Mater. Sci. Technol.*, 1997, vol. 13, pp. 49-55.
20. D. Hall and J. Worobec: in *Phase Transformations During the Thermal/Mechanical Processing of Steel*, E.B. Hawbolt and S. Yue, eds., The Metallurgical Society of CIM, Montreal, 1995, pp. 305-16.
21. Z. Chen, M.H. Loretto, and R.C. Cochrane: *Mater. Sci. Technol.*, 1987, vol. 3, 836-44.
22. R.G. Baker and J. Nutting: in *Precipitation Processes in Steels*, The Iron and Steel Institute, London, 1959, pp. 1-21.
23. M. Umemoto, A. Hiramatsu, A. Moriya, T. Watanabe, S. Nanba, N. Nakajima, G. Anan, and Y. Higo: *Iron Steel Inst. Jpn. Int.*, 1992, vol. 32, pp. 306-15.
24. J. Bošansky, D.A. Porter, H. Åström, and K.E. Easterling: *Scand. J. Metall.*, 1977, vol. 6, pp. 125-31.
25. *JCPDS–International Center for Diffraction Data*, Version 2.12, JCPDS-ICDD, Swarthmore, PA, 1991.
26. M.T. Miglin, J.P. Hirth, A.R. Rosenfeld, and W.A.T. Clark: *Metall. Trans. A*, 1986, vol. 17A, pp. 791-98.
27. P. Choquet, P. Fabrègue, J. Giusti, B. Chamont, J.N. Pezant, and F. Blanchet: in *Mathematical Modelling of Hot Rolling of Steels*, S. Yue, ed., The Metallurgical Society of CIM, Montreal, 1990, pp. 34-43.
28. E. Nes: *Progr. Mater. Sci.*, 1997, vol. 41, pp. 129-93.
29. H.J. Frost and M.F. Ashby: *Deformation-Mechanisms Maps*, Pergamon Press, Oxford, United Kingdom, 1982.
30. T. Gladman: *Mater. Sci. Technol.*, 1999, vol. 15, pp. 30-36.
31. D. Hull and D.J. Bacon: *Introduction to Dislocations*, 3rd ed, Pergamon Press, Oxford, United Kingdom, 1984.
32. M.F. Ashby: *Cambridge Materials Selector*, Software Version 2.02, Granta Design Ltd., Cambridge, UK, 1994.
33. L.M. Brown and R.K. Ham: in *Strengthening Methods in Crystals*, A. Kelly and R.B. Nicholson, eds., John Wiley & Sons, New York, NY, 1971, pp. 12-135.
34. T. Gladman: *The Physical Metallurgy of Microalloyed Steels*, Institute of Materials, London, 1997.
35. A.J.E. Foreman and M.J. Makin: *Can. J. Phys.*, 1967, vol. 45, pp. 511-17.
36. K.A. Taylor: *Scripta Metall. Mater.*, 1995, vol. 32, pp. 7-12.
37. M. Vivas, P. Lours, C. Levaillant, A. Couret, M.J. Casanove, and A. Coujou: *Mater. Sci. Eng. A*, 1997, vols. A234-A236, pp. 664-67.